

SUPPORTING INFORMATION

**Microwave-Assisted Solution-Liquid-Solid Synthesis of
Single-Crystal Copper Indium Sulfide Nanowires**

Galyna Krylova,¹ Halyna Yashan,¹ John G. Hauck,² Peter C. Burns,^{1,3}

Paul J. McGinn,² Chongzheng Na^{1,*}

¹Department of Civil and Environmental Engineering and Earth Sciences, University of

Notre Dame, 156 Fitzpatrick Hall, Notre Dame, Indiana 46556.

²Department of Chemical and Biomolecular Engineering, University of

Notre Dame, 182 Fitzpatrick Hall, Notre Dame, Indiana 46556.

³Department of Chemistry and Biochemistry, University of Notre Dame,

251 Nieuwland Science Hall, Notre Dame, Indiana 46556.

*Corresponding author: chongzheng.na@gmail.com.

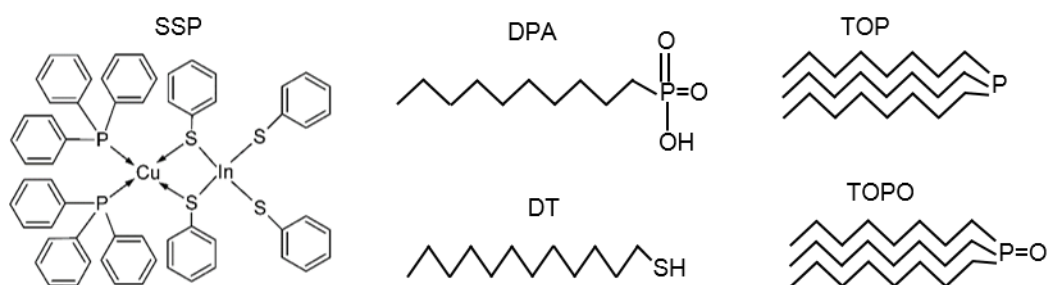


Figure S1. Structures of single-source precursor (SSP), decylphosphonic acid (DPA), dodecanethiol (DT), trioctylphosphine (TOP), and trioctylphosphine oxide (TOPO).

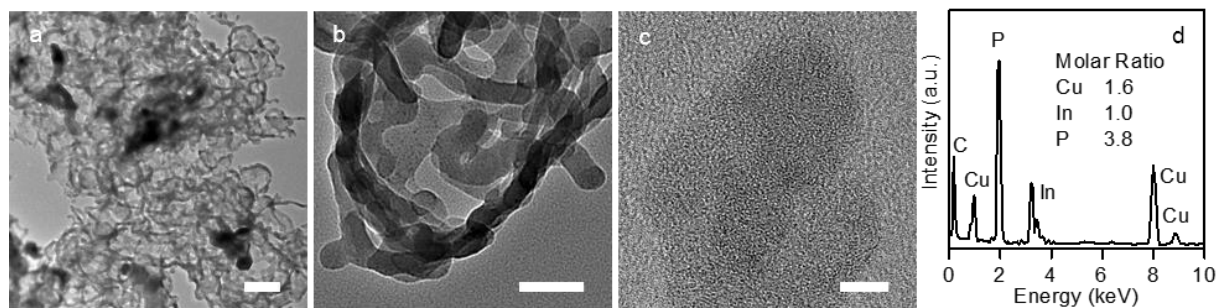


Figure S2. Poorly crystallized phosphide nanowires formed by irradiating 1 mL reactive solution containing BiCl_3 , SSP, DPA, acetone, TOP at a molar ratio of 0.002:1:4:13.3:52 at 300 °C for 5 min. (a – c) Transmission electron micrographs. (d) Energy dispersive X-ray spectrum with estimates of molar ratios of Cu, In, and P. Scale bars: *a*, 200 nm; *b*, 50 nm; *c*, 5 nm.

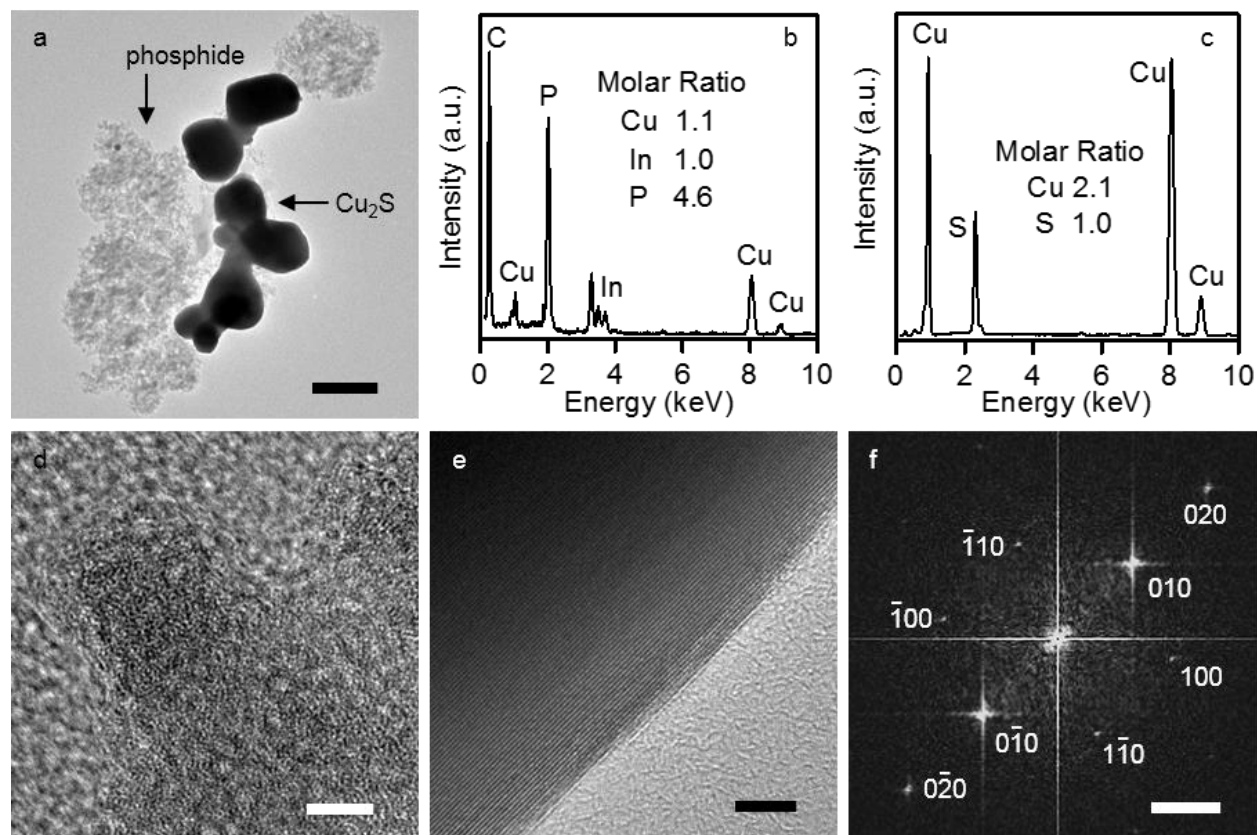


Figure S3. Amorphous phosphide and crystalline chalcocite (Cu_2S) particles formed by HISLS with 1 mL of the precursor solution used in MASLS synthesis, containing BiCl_3 , SSP, TOP, DT, acetone, and TOPO at a molar ratio of 0.002:1:2:4:13.6:50. The synthesis temperature and duration were ca. 291°C and 5 min. (a) Transmission electron micrograph (TEM) of the product mixture. (b, c) Energy dispersive X-ray spectra of amorphous phosphide and Cu_2S particles. (c, e) TEMs of amorphous phosphide and Cu_2S particles. (f) Fast Fourier transform of *e*, revealing the electron diffraction patterns of chalcocite Cu_2S viewed in the $[001]$ direction. Scale bars: *a*, 500 nm; *d* and *e*, 5 nm; *f*, 2 nm^{-1} .

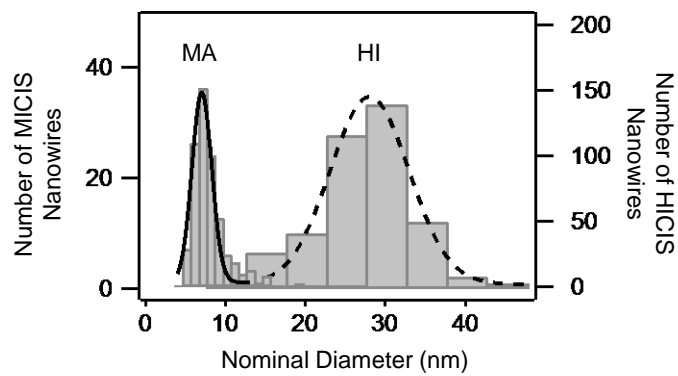


Figure S4. Diameter histograms for CuInS₂ nanowires synthesized by microwave-assisted (MA) and hot-injection (HI) SLS. The diameters were measured from TEM images taken with 450 nanowires (MA data are measured from different batches).

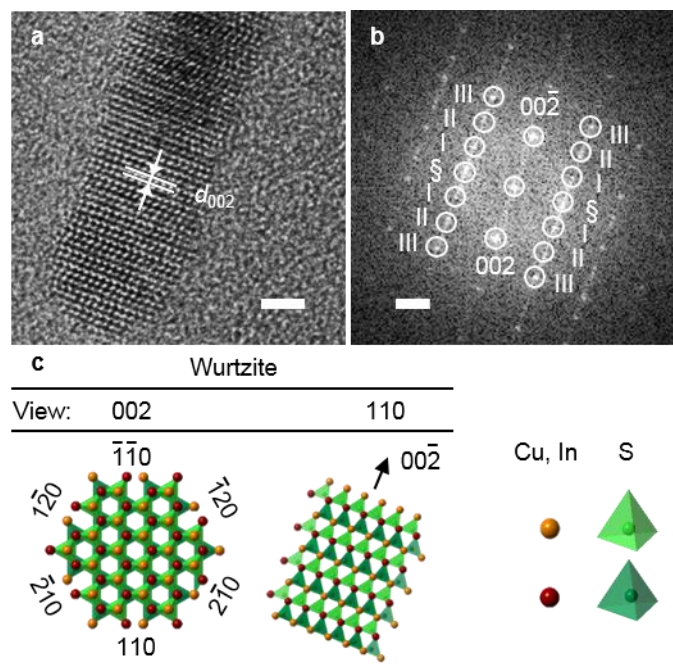


Figure S5. TEM, FFT, and truncated structure of wurtzite impurity produced by MASLS. Scale bars: *a*, 2 nm; *b*, 2 nm⁻¹. Symbols: O, simulated diffraction patterns; †, 0 $\bar{2}4$, $\bar{2}04$, or $\bar{2}20$; ‡, $13\bar{2}$, $31\bar{2}$, $\bar{1}16$, or $1\bar{1}6$; §, $\bar{1}10$, $\bar{1}00$, $0\bar{1}0$; *n* = I, II, III, $\bar{1}1n$, $1\bar{1}\bar{n}$, $0\bar{1}n$, $0\bar{1}\bar{n}$, $10n$, or $\bar{1}0\bar{n}$.

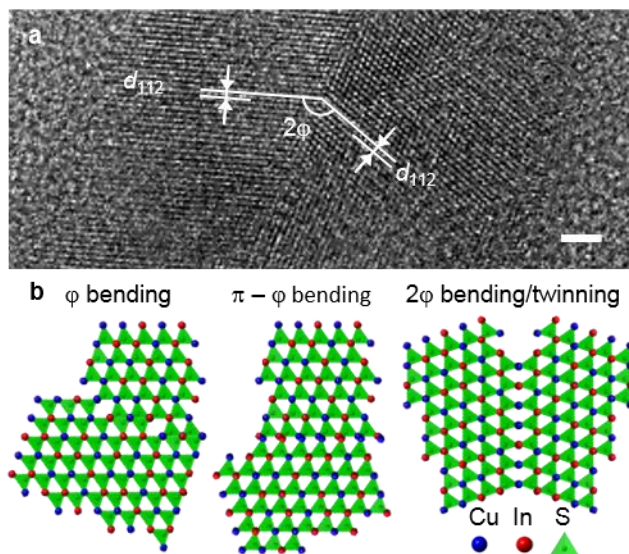


Figure S6. Bending and twinning of CuInS₂ nanowires synthesized by HISLS. (a) High resolution transmission electron micrograph (scale bar: 2 nm). (b) Model representation. In the cubic-close packed chalcopyrite structure, there are 8 equivalent {112} planes, resulting in three scenarios with bending/twinning angles of ϕ , $\pi - \phi$, and 2ϕ with a theoretical value of $\phi = 70.5^\circ$. All three scenarios are evident in TEM images of HI nanowires (cf. Figure 1a), from which we estimate $\phi = 68(\pm 4)^\circ$.

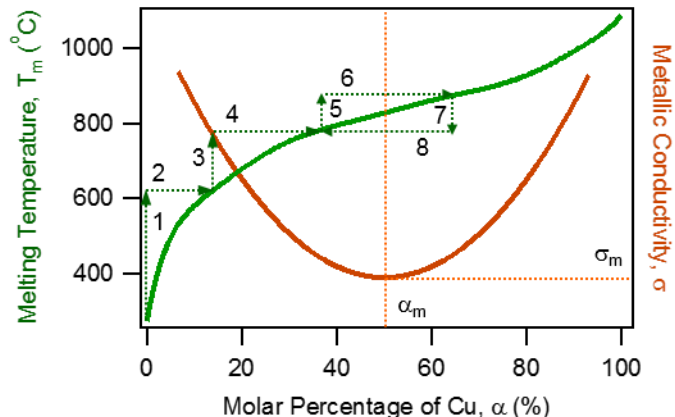


Figure S7. Relationships of melting temperature and electrical conductivity with the composition of Bi-Cu alloy. The composition-temperature data are from Chakrabarti and Laughlin.¹ The composition-conductivity relationship is drawn schematically based on measurements made for Cu alloys with Al, Au, Ni, Pd, and Zn by Ho et al.² The green arrows illustrate the steps leading to the incorporating of Cu under microwave irradiation on the composition-temperature curve. The dotted line in orange marks the lowest conductivity at the composition with equimolar Bi and Cu. We propose that the unique composition of solidified catalyst nanoparticles with a molar ratio of Bi:Cu \approx 1:1, results from the unique relationships of melting temperature T_m and electrical conductivity σ with alloy composition. The nanoparticles and the corresponding liquid nanodroplets are sufficiently small (< 100 nm in diameter) for microwaves to completely penetrate them (penetration depth > 1 μ m). The absorption of microwave power is inversely related to the square root of σ :²

$$P = H_{\text{rms}}^2 \sqrt{\frac{\omega\mu}{2\sigma}} \quad (\text{S1})$$

where H_{rms} is the root-mean-square value of the magnetic field strength, ω is the angular frequency of the microwave irradiation, and μ is the permeability. As the Bi nanodroplets are heated (Step 1 in Fig. S1), they incorporate Cu (Step 2). As the Cu percentage α increases, σ decreases so that P increases. As a result, T_m increases further (Step 3), which further increases α (Step 4). Repeating these steps keeps increasing both T_m and α until the system approaches the minimum point of the composition-conductivity relationship (the orange dotted line in Fig. S1). A further increase of temperature (Step 5) leads to the cross-over of the minimum conductivity point defined by σ_m and $\alpha_m \approx 50\%$ (Step 6), which now produces an alloy with an increased conductivity and thus reduced ability to absorb microwaves. As a result, T_m decreases (Step 7) and Cu precipitates from the nanodroplets, which reduces α (Step 8). Now, the system crosses back over the conductivity minimum and circulates around it by following Step 5 – 8. The presence of a minimum conductivity prevents thermal runaway that could result from the overheating of metallic catalysts by microwave irradiation.

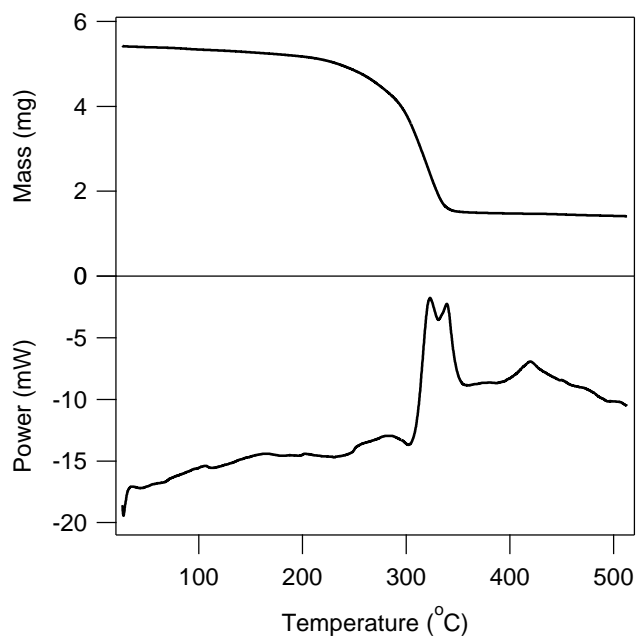


Figure S8. Decomposition of single-source precursor analyzed by (a) thermogravimetric analysis and (b) differential scanning calorimetry. Temperature ramp rate: $10\text{ }^{\circ}\text{C min}^{-1}$. The decomposition occurs from approximately $200\text{ }^{\circ}\text{C}$ but only becomes significant near $300\text{ }^{\circ}\text{C}$.

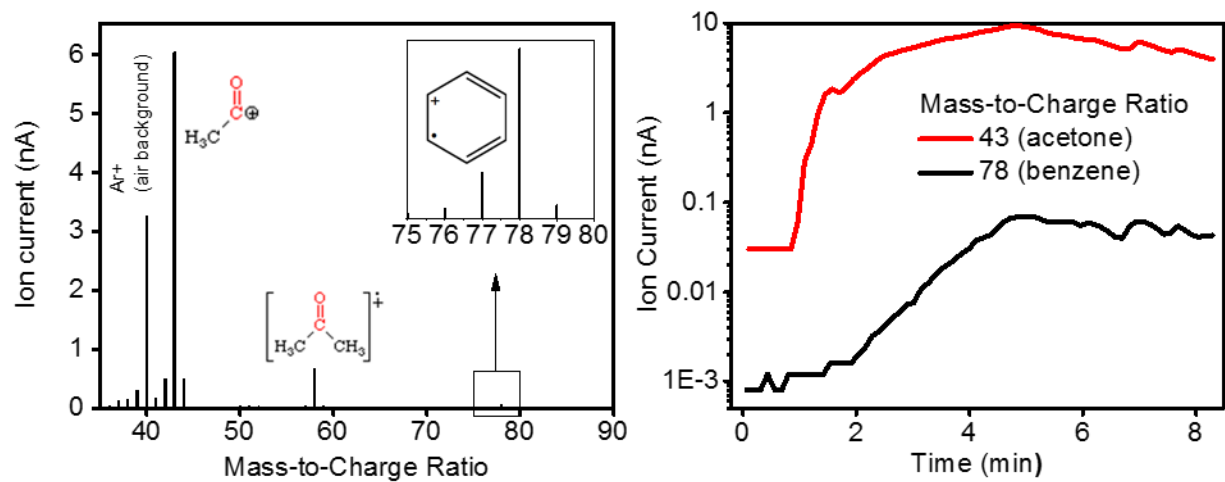


Figure S9. Mass spectrometry measurements of vapors produced in MASLS. (a) Mass spectrum at 5 min. (b) Evolution of acetone and benzene with time.

References

1. D. J. Chakrabarti and D. E. Laughlin, *Bull. Alloy Phase Diagr.*, 1984, **5**, 148-155.
2. C. Y. Ho, M. W. Ackerman, K. Y. Wu, T. N. Navill, R. H. Bogaard, R. A. Matula, S. G. Oh and H. M. James, *J. Phys. Chem. Ref. Data*, 1983, **12**, 183-321.